Longitudinal dispersion in natural channels: 2. The roles of shear flow dispersion and dead zones in the River Severn, U.K.

P. M. Davis, T. C. Atkinson, T. M. L. Wigley

Hydrology and Earth System Sciences, 4(3), *355–371* (2000) © EGS

Hydrology & Earth System Sciences

Longitudinal dispersion in natural channels: 2. The roles of shear flow dispersion and dead zones in the River Severn, U.K.

P.M. Davis[2], T.C. Atkinson[1,2] and T.M.L. Wigley[2,3]

[1]Groundwater Tracing Unit, Department of Geological Sciences, University College London, London WC1E 6BT, U.K.
[2]School of Environmental Sciences, University of East Anglia, Norwich NR4 7TJ, U.K.
[3]National Center for Atmospheric Research, P.O. Box 3000, Boulder CO 80307-3000, U.S.A.
e-mail for corresponding author: t.atkinson@ucl.ac.uk

Abstract

The classical one-dimensional advection-diffusion equation (ADE) gives an inadequate description of tracer cloud evolution in the River Severn, U.K. A solute transport model incorporating the effects of tracer storage in dead zones is presented in which the channel is conceived as being divided into two parallel regions. The *bulk flow region* occurs in the central part. Its longitudinal dispersive properties are described by the ADE. Adjacent to this, an additional cross-sectional area is defined in which tracer can be stored temporarily in regions of slowly moving water called *dead zones*. Exchange between the two regions follows a first order rate equation. Applying the model to the River Severn shows that a dispersing cloud's evolution occurs in two distinct stages with a rapid transitional phase. Initially, shear-dispersion is dominant while the tracer particles mix fully over the bulk flow. Once this has occurred, dead zone storage accounts well for the non-Fickian evolution of the cloud. After the transitional phase the dead zone storage mechanism clearly dominates over shear-dispersion. Overall, the combined shear flow dispersion–dead zone model (D-DZM) provides a much better, physically consistent description of the tracer cloud's evolution than the simple classical ADE approach can do alone.

Keywords: Channels; dispersion; dead zones; tracers; River Severn

Introduction

This paper deals with the longitudinal dispersion of a passive, conservative tracer as it is transported and diluted by the flow in a natural river channel. Experimental data on tracer cloud evolution over 14 km in the River Severn, U.K., was introduced in a companion paper (Atkinson and Davis, 2000). Here a detailed analysis is presented of these data in terms of two dispersion processes–shear flow dispersion within the main channel, and tracer storage, retention and release from regions of static or slowly moving water known as *dead zones*. The structure of the paper is as follows. Firstly, it is shown that the classical approach to longitudinal dispersion by advection combined with turbulent shear, first developed by Taylor (1954), does not provide an adequate description of the River Severn data. The possible reasons for this failure are discussed and the omission of dead zone processes is identified as a likely cause before an analytical model is developed incorporating both sets of processes. This is then applied to the River Severn data; the inclusion of dead zone processes provides a physically consistent description of the tracer cloud's evolution, which is greatly superior to the classical model. By means of this analysis, different periods in the cloud's evolution can be identified; firstly, shear flow dispersion dominates and later dead zone dispersion becomes predominant. This affords new insights into the longitudinal dispersion process in natural channels.

Application of Taylor's theory to the River Severn data

TAYLOR'S SOLUTION OF THE ADVECTION-DISPERSION EQUATION

Conventionally, the approach to the dispersion problem in natural channels has been based upon Taylor's (1921) classical analysis of diffusion by continuous movements, which was subsequently applied to the analysis of continuous turbulent shear-dispersion in a uniform circular pipe (Taylor, 1954). Provided sufficient time has elapsed since mass injection, this theory leads to the one-dimensional advection-dispersion equation (ADE) for cross-

sectionally averaged concentration C and velocity U,

$$\frac{\partial C}{\partial t} + U\frac{\partial C}{\partial x} = K\frac{\partial^2 C}{\partial x^2} \quad (1)$$

where K is the shear-dispersion coefficient.

Equation (1) is a limiting case that is applicable only after the solute has been dispersing for a period of time in excess of the Lagrangian time scale. This is the time required for tracer particles to lose memory of their initial, position-dependent velocity, or alternatively is the time scale over which the Lagrangian streamwise velocity of an individual tracer particle can be regarded as a stationary random function with zero mean. It is also the time required for tracer particles to sample fully the variation in advective velocities over the flow field.

For an instantaneous injection extending over the cross-section at $x = 0$, $t = 0$ a solution to the one-dimensional ADE is given by:

$$C(x,t) = \frac{M}{2A(\pi Kt)^{1/2}}\exp\left[-\frac{(x-Ut)^2}{4Kt}\right] \quad (2)$$

Equation (2) states that the distributions of C when sampled as a function of t at some longitudinal distance x will be asymmetrical about $t = x/U$. This reflects the fact that the parts of the cloud which pass x later have been dispersing for a longer time than those which pass x first. However, if the rate at which the tracer cloud is advected past x is rapid compared to the rate of dispersion, then there will be negligible evolution over the sampling period and Eqn. (2) will be an approximately Gaussian function of t. This is known as the frozen cloud approximation.

It has long been known that Taylor's limiting theory, Eqn. (1), is an inadequate description of the mechanisms present in natural channels (Elder, 1959; Fischer, 1967; Nordin and Sabol, 1974; Day and Wood, 1976). Empirical data show initial development of a pronounced skewness in the trailing limb that is much greater than can be accounted for by the frozen cloud approximation or by the continued dispersion by shear flow as the cloud passes the sampling point. The assumption that these skewed concentration distributions will eventually converge to equations of the form (2) is not supported by empirical observations in natural channels.

This paper examines the origin of the systematic deviations of empirical concentration distributions from Taylor's limiting theory and attributes them to the temporary retentive effects of regions of tracer storage. These so called 'dead zone' regions have been the subject of ongoing discussion (Schnelle *et al.*, 1967; Hays and Krenkel, 1968; Patterson, 1968; Thackston and Schnelle, 1970; Valentine and Wood, 1977, 1979a, b; Nordin and Troutman, 1980; Bencala and Walters, 1983; Beer and Young, 1983; Legrand-Marcq and Laudelout, 1985; Purnama, 1988a, b; Wallis *et al.*, 1989; Denton, 1990) but surprisingly few of these studies have discussed the nature and role of dead zones in natural channels, nor analysed their influence on empirical data from tracer experiments in rivers.

APPLICATION OF THE ADVECTION-DISPERSION EQUATION TO DATA FROM THE RIVER SEVERN

Atkinson and Davis (2000) give a detailed description of the 13775 m reach of the River Severn used for a tracer experiment. The channel dimensions of width (W), average depth (D) and cross-sectional area (A) showed considerable variability from one cross-section to another, the cross-sections being spaced ~100 m apart. On distance scales greater than ~100 m, however, the variability was much less, and the whole reach is statistically of uniform depth. Statistically it is somewhat non-uniform with respect to both width and cross-sectional area, as the downstream part of the reach tends to be wider and have a larger area than the upstream part. The difference is not great, however. This variability is on the ~10 km scale and appears much smaller than that on the ~100 m scale. Details are given by Atkinson and Davis (2000). The overall mean cross-sectional area and standard deviation is $A = (12.06 \pm 3.76)\ \mathrm{m}^2$, while $D = (0.53 \pm 0.18)$ m and $W = (23.8 \pm 6.6)$ m. Overall, the channel appears to be near enough to statistical uniformity for it to be expected that an equation such as the one-dimensional ADE (i.e. Eqn. (1)) would be applicable over distance scales of ~1000 m or more. At these larger scales the irregularities of the channel should be treatable as "noise", so that the classical approach of assuming a truly uniform channel is appropriate. This point is important in the analysis which follows, because an effectively uniform channel should display statistically constant shear flow dispersion. Therefore, it may be expected *a priori* that the shear-dispersion coefficient K in Eqn. (1) will have a constant value over all distances from the injection point. If fitting the ADE to tracer data from such a near-uniform reach as that on the River Severn gives values of K which change significantly with distance, then the ADE itself does not provide a complete description of the dispersion processes which actually occur.

Chatwin (1971) proposed a method to provide information on the deviations, or otherwise, of concentration-time distributions from Eqn. (2) which is first linearized,

$$\left[t\log(A^*/Ct^{1/2})\right]^{1/2} = \left(\frac{x}{2K^{1/2}} - \frac{Ut}{2K^{1/2}}\right) \quad (3)$$

where A^* is introduced for $M/2A(\pi K)^{1/2}$. If the concentration distributions are symmetrical, then at $x = Ut$, $C = C_p = A^* t_p^{-1/2}$ giving $A^* = C_p t_p^{1/2}$ where C_p is the peak concentration and t_p is the time to the peak concentration. It has been shown by Day (1975) that calculating A^* in this manner leads to only very small errors for asymmetrical distributions. In addition, Chatwin (1971) states that only those points near $t = x/U$ are sensitive to the value of A^* used.

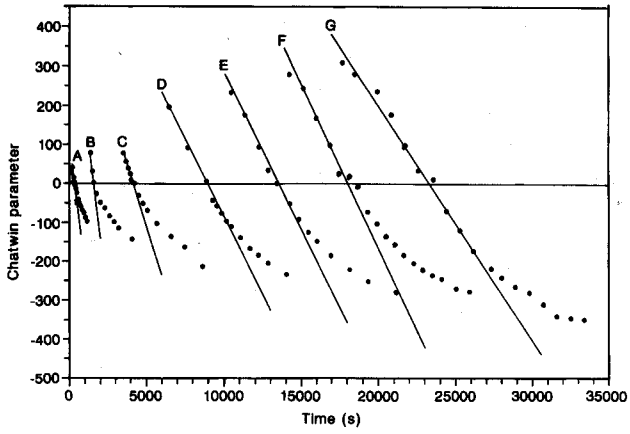

Fig. 1. *Application of Chatwin's (1971) analysis. The solid lines are regression lines fitted to the leading edges of the tracer distributions.*

The left hand side of Eqn. (3), called the Chatwin parameter, is calculated and plotted against time. If the graph is a straight line Eqn. (3) is an appropriate model, for which the values of U and K can be determined from the slope and intercept.

The results of applying Chatwin's (1971) analysis are shown in Fig. 1. The non-linearity exhibited by the data sets for all stations show that none of the empirical tracer distributions can be accounted for by Eqn. (2).

For times less than approximately x/U, which represent the leading parts of the tracer distributions, the plots are linear and this part of each curve can be described by the Gaussian equation,

$$C = A^* t^{-1/2} \exp\left[-\frac{(x - U_c t)^2}{4K_c t}\right] \qquad (4)$$

where the subscript in K_c and U_c indicates that these are estimates based on Chatwin's (1971) analysis. The fitted values of K_c and U_c are shown in Table 1. In Fig. 2 the velocities U_c are plotted against the average velocity upstream of each station given by Atkinson and Davis (2000, Table 2). The shear-dispersion coefficients K_c are plotted against distance in Fig. 3.

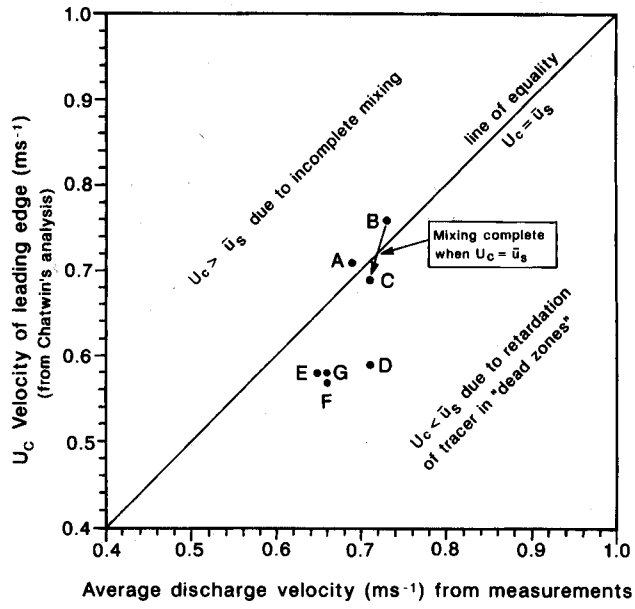

Fig. 2. *Upstream average current-metered discharge velocity $\bar{u}_s$ versus Chatwin-fitted velocity of the leading edge of the tracer distribution, U_c. The solid line represents $\bar{u}_s = U_c$, and the arrowed box shows the movement of the tracer cloud's velocity across the line, which indicates the Lagrangian timescale.*

Even if the non-Gaussian nature of the trailing edges is ignored, the downstream increase in K_c shown in Fig. 3 implies that the tracer cloud does not evolve according to Eqn. (2). Thus, Taylor's limiting theory fails the *a priori* test of constancy of dispersion parameters in a statistically almost uniform channel. This suggests that it will also prove inadequate to describe the statistical properties of the evolving cloud.

THE ADVECTION-DISPERSION EQUATION AND THE STATISTICAL PROPERTIES OF THE EVOLVING CLOUD

Figure 4a shows the peak concentrations of the empirical data as a function of downstream distance. Equation (2)

Table 1. Values of K_c and U_c from Chatwin's (1971) analysis applied to the River Severn.

Station	$K_c(m^2s^{-1})$	$U_c(ms^{-1})$
A	1.26	0.71
B	1.42	0.76
C	7.88	0.69
D	14.07	0.59
E	12.72	0.58
F	16.10	0.57
G	27.78	0.58

Table 2. Optimal solutions (α_o) of the D-DZM with corresponding values of $F(\alpha_o)$ for the River Severn.

Station	K_o (m^2s^{-1})	χ_o	τ_o (s)	$F(K_o, \chi_o, \tau_o)$
A	2.461	4.044	2920	0.0061
B	3.358	2.713	4197	0.0187
C	7.164	3.118	5077	0.0008
D	2.387	2.144	1260	0.0059
E	0.053	2.111	4797	0.0612
F	0.079	2.098	2973	0.0422
G	0.105	2.166	3046	0.0272

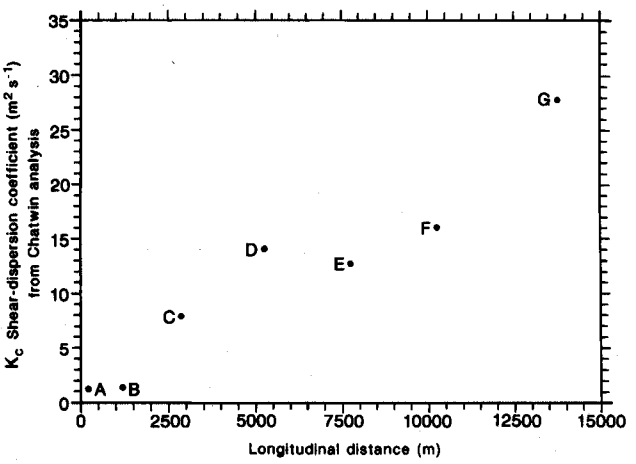

Fig. 3. *Shear-dispersion coefficients obtained from Chatwin's (1971) analysis, K_c versus longitudinal distance.*

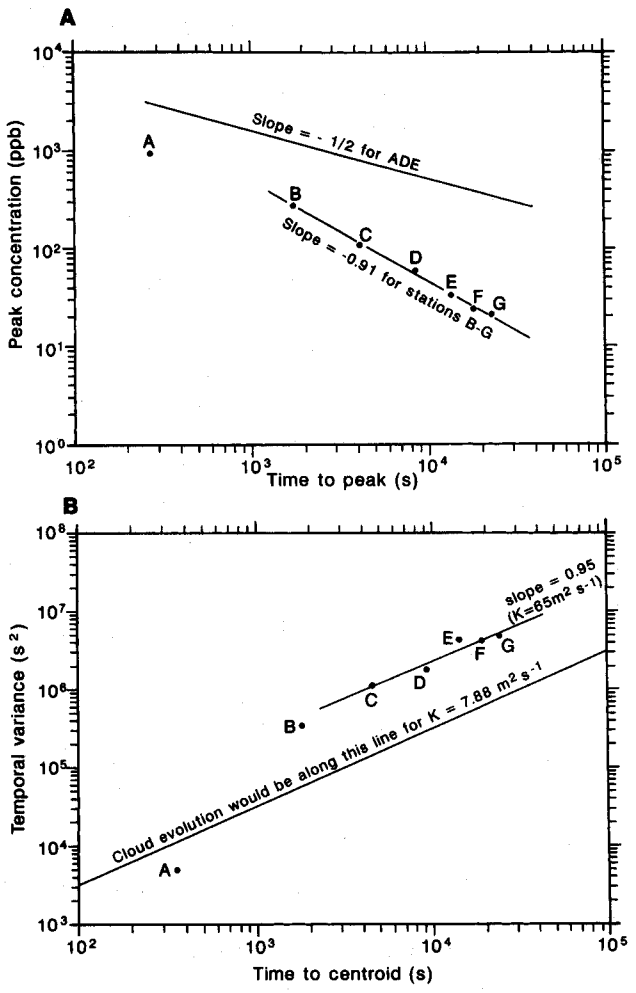

Fig. 4. *(a) Peak concentration versus time-to-peak (closed circles) together with the peak concentration decay rate predicted by Eqn. (2) (upper line). Lower line is a regression through stations B to G. (b) Temporal variance, σ_t^2 of the cloud (closed circles) against time to cloud centroid, with regression line through stations C to G (upper line). Lower line shows expected evolution of the cloud with $K = 7.88\ m^2 s^{-1}$ (i.e. value for station C) according to Eqn. (2).*

predicts that C_p will decay at a rate proportional to $t^{-1/2}$ i.e. with the gradient shown by the straight line. The rate of decay of the empirical peak concentrations is seen to be continually greater than $t^{-1/2}$ and at no time approaches it. Consequently, Eqn. (2) is increasingly inaccurate in predicting C_p for stations further downstream, unless the value of K is continually increased so as to force the ADE to mimic the data, as has been done in deriving the values of K_c in Fig. 3.

Figure 4b shows the temporal variances σ_t^2 of the tracer distributions given by

$$\sigma_t^2 = \frac{\int_{-\infty}^{\infty}(t-\bar{t})^2 C dt}{\int_{-\infty}^{\infty} C dt} \qquad (5)$$

where $\bar{t}$ is the time to the centroid of the concentration distribution. After a sufficiently long time period has elapsed for Eqn. (2) to become applicable, Taylor's limiting theory predicts that $\sigma_x^2 = 2Kt$. By making use of the frozen cloud approximation, the spatial variance σ_x^2 can be converted to a temporal variance via $\sigma_t^2 = \sigma_x^2/U_c^2$. Predictions based on Eqn. (2) will therefore give rise to σ_t^2 increasing linearly with time, i.e. with a gradient of unity on logarithmic axes.

The upper sloping line shown in Fig. 4b is a regression through the σ_t^2 values of the data from station C through to station G. It has a correlation coefficient of 0.96 and a gradient of 0.95. Thus, the values of σ_t^2 increase at a rate that is very nearly linear with time, just as Eqn. (2) predicts. This means that the temporal variance of the tracer cloud from station C downstream evolves at a constant rate in accordance with the Taylor theory. However, the value of K required is 65 assuming a value of U_c of $0.58\ m.s^{-1}$ [Stations D-G, Table 1]. This is a much greater dispersion coefficient than any of those in Table 1 and Fig.3. Linearity in variance with time is a necessary but not a sufficient criterion for Eqn. (2) to be a valid description of the evolving cloud.

Later in this paper, it is shown that the Lagrangian timescale was passed when the peak and leading edge of the cloud lay between stations B and C. Thus, station C is the first at which the conditions assumed in Taylor's limiting solution of the ADE can be expected to apply. The value of K_c at station C is $7.88\ m^2 s^{-1}$. The lower sloping line on Fig. 4b indicates the expected evolution of the cloud according to the ADE if K were constant at this value. It is clear that this line cannot, even to a first approximation, account for the values of σ_t^2 at station C or any other downstream station. This shows that the true dispersive processes affecting the cloud are much more effective than suggested by the values of K_c which are derived from only the leading edges and peaks of the tracer distributions. In their entirety, the tracer curves have a much greater temporal variance associated with the non-Gaussian, asymmetrical trailing limbs that were not taken into account in deriving K_c.

Another feature of the ADE model when fitted by the Chatwin (1971) method is that it does not preserve mass balance. There are various ways in which this shortcoming can be expressed. If the Chatwin-derived values for A^* and K_c are used, then their ratio can be used to calculate an implied mass injected which is invariably smaller than the true mass. This, of course, reflects the operation of an unaccounted process which transfers mass from the main part of the cloud into a growing tail. If, on the other hand, one adopts the value of $K = 65\ m^2s^{-1}$ required to describe the evolution of the temporal variance, the mass of dye is overestimated at all stations except F and G.

Possible explanation for non-Gaussian behaviour

Systematic inconsistencies and discrepancies between the one-dimensional ADE and actual cloud evolution are well known in empirical data and have been reported by Fischer (1967), Godfrey and Frederick (1970), Nordin and Sabol (1974), and Nordin and Troutman (1980), but not always comprehensively explored.

Taylor (1954) confirmed his theory for turbulent flow by experiments in a smooth-walled uniform pipe with sampling at times which he judged to be sufficiently long for Eqn. (2) to apply. However, at low Reynolds numbers he observed similar deviations from his theory to those described above. These he attributed to the development of a significant laminar sublayer which is not considered in his theory. Taylor's limiting theory has successfully been extended to uniform smooth- and rough-walled laboratory flumes, a natural stepping-stone in the progression to river flows (Fischer, 1966; Sayre and Chang, 1968; Valentine and Wood, 1979a). Here however, the effects of the sublayer become important, increasing the time required for the theory to become applicable and the apparent value of the shear-dispersion coefficient.

Sullivan (1971) describes the dispersion process in a uniform shear flow in terms of three stages. The first stage is not important here as it relates to the time period before cross-sectional mixing has been established. The second stage begins when tracer particles have become well mixed over the bulk flow region but before a significant flux of particles into the viscous sublayer has occurred. In this stage, tracer particles enter the sub-layer for the first time and are retained there before being released by diffusion back into the main flow. Cross-sectionally averaged concentrations for particles outside the viscous sublayer are Gaussian and described by the value of the shear-dispersion coefficient determined by conditions in the main flow. Complete cross-sectional average profiles (including the sublayer) exhibit tailing. The second stage evolves very slowly into a third stage (Chatwin, 1973; Dewey and Sullivan, 1977) which is reached when the tracer particles have had time to sample the entire flow field, including the viscous sublayer. Sullivan (1971) suggests that this is the time period when Taylor's limiting theory is a sufficient description of the dispersion process.

In an explanation of the non-Gaussian behaviour of empirical data from natural channels, many authors hold the view that the retention of tracer in low velocity regions (caused for example by irregularities in cross-sectional geometry, embayments in the banks, or the porosity of coarse gravels on the bed) are analogous to the sublayer in uniform laboratory flumes. It is concluded by such authors that the reason Eqns. (1) and (2) appear inadequate is because the tracer has not been dispersing for a sufficiently long time period. It is implicit in this view that eventually the concentration distributions will be described adequately by Eqn. (1) when a stage analogous to the third stage described by Sullivan (1971) is reached.

The main failing of this explanation is that no data from natural channels has shown a reduction in skewness that might be associated with the trend towards fitting Eqn. (2). The same is not true, however, for the longitudinal dispersion process in laboratory flumes, even with idealised dead zones. For natural channels deviations in the empirical data from Eqn. (2) become greater at increasing times (distances) from the point of mass injection.

The reason for the inadequacy of Taylor's limiting theory therefore lies in the variation in tracer concentration over the cross-section. Visual observation of the longitudinal dispersion process in natural channels provides information on this e.g. the descriptions and photographs in Fischer (1967, 1968) and Rutherford *et al.* (1980). These publications show that, for times greater than the time to the peak concentration, the tracer particles are concentrated near the boundaries of the channel. The tails of the concentration distributions decay more slowly than Gaussian distributions as a result of the temporary entrapment of tracer particles in regions of dead zone storage. This evidence suggests that the reason for the inadequacy of Eqn. (2) is associated with the retentive properties of boundary regions. It is proposed here that Eqn. (2) is applicable (after a sufficiently long time) to describe the shear-dispersive properties of the bulk flow regime, and that the non-Gaussian behaviour arises as a consequence of the dead zone storage mechanism. Previous studies have shown that the dispersive properties of dead zones can vastly increase the dispersion and skewness in models (Aris, 1959; Thackston and Schnelle, 1970; Valentine and Wood, 1979a, b; Purnama, 1988a, b; Denton, 1990).

In the River Severn data, the discharge velocity $\bar{u}_s$ is a property of the bulk flow regime. Dead zones were not included in the measured cross-sections which were chosen for their regularity and lack of backwaters. Thus, the current-metered values of discharge and velocity do not take into account the very low longitudinal velocities adjacent to the channel boundaries. Prior to the time period when the tracer particles have had time to sample all the advective velocities over the bulk flow regime, U_c will be greater than

$\bar{u}_s$ as the cloud will be concentrated in the faster-moving parts of the main flow. A distance scale for cross-sectional mixing over the bulk flow regime can be determined from the comparison of U_c and $\bar{u}_s$ in Fig. 2. When $U_c = \bar{u}_s$ the ensemble of tracer particles in the leading edge of the cloud has an average velocity equal to the discharge velocity. This occurs only when tracer particles have sampled all the advective velocities over the bulk flow regime.

In the dispersion model to be presented, the Lagrangian time scale is defined in terms of cross-sectional mixing over the bulk flow regime and not the entire flow field. Figure 2 shows that the longitudinal distance required for $U_c/\bar{u}_s$ to be unity occurs between 1175 m (station B) and 2875 m (station C). This estimate of the Lagrangian scale suggests that for stations C through G the tracer will have sampled all parts of the bulk flow regime and that Eqns. (1) and (2) should apply. The facts that Eqn. (2) does not in fact describe the evolution of the cloud and that $U_c < \bar{u}_s$ downstream of station C confirm the previous conclusion that an important storage mechanism has been neglected. Dead zone storage can account for the entrapment and subsequent slow release of tracer particles stored in local areas of the channel boundary that are partially isolated from the bulk flow, and are assumed to have little or no net longitudinal advective velocity.

It can be seen in Fig. 2 that the velocity of the quasi-Gaussian leading edge of the cloud becomes progressively less than the discharge velocity, eventually settling to around 88% of its value in stations E, F and G. This may be explained by the retention of tracer particles from both the leading edges and trailing parts of the tracer cloud, when sufficient time has elapsed for most particles in the cloud to have passed through the dead zone storage mechanism at least once.

The shear flow dispersion-dead zone model (D-DZM)

For channelled flows Hays (1966) and Hays and Krenkel (1968) were the first to consider two-zone models where non-Gaussian behaviour arises from the retentive effects of dead zones. Subsequently, other authors have taken this approach (Thackston and Schnelle, 1970; Valentine and Wood, 1977; Nordin and Troutman, 1980; Bencala and Walters, 1983; Legrand-Marcq and Laudelout, 1985; Purnama, 1988a, b; Denton, 1990). Appendix B indicates related mathematical work in other fields.

MODEL DEVELOPMENT

This section develops a model incorporating both the classical shear flow dispersion of Eqn. (1) and the dead zone mechanism discussed above. It is, therefore, termed the Dispersion–Dead Zone Model (D-DZM). The channel is separated into two parallel regions, one with bulk flow in which the cross-sectionally averaged concentration is C, the other being the dead zone storage region with uniform concentration (at a single position, x) of C_s. After an appropriate time to allow cross-sectional mixing following injection, it is assumed that Eqn. (1) will describe the longitudinal transport and dispersion of tracer in the well mixed bulk flow region. The quasi-Gaussian leading edges of the tracer curves in Fig. 1 support the view that shear-dispersion does indeed play a role. Adjacent to the core part of the channel a dead zone area is defined with an effective cross-sectional area A_s. Transfer of tracer between the dead zone and the bulk flow is described by a first-order mass transfer. The actual physical mechanism involved may depend on the type of dead zone, e.g. advection into backwaters by means of occasional random eddies; diffusion either by molecular motion or by frequent small scale eddying at the entrance to dead zones; molecular diffusion into the pore space of a granular bed; entrapment of tracer in permanent eddies behind obstructions and so on. It is assumed in the D-DZM that a single type of dead zone predominates, that the tracer within it is well mixed, and that dead-zone effects can be characterised by a single transfer velocity coefficient. One might object that this is excessively crude by comparison with physical reality, but it leads to simplicity of mathematical formulation and tractability, which a more complicated model might not do.

By applying the principle of mass conservation to an incremental volume the following coupled partial differential equations can be derived. For the bulk flow region,

$$\frac{\partial C}{\partial t} + U\frac{\partial C}{\partial x} - K\frac{\partial^2 C}{\partial x^2} = -\frac{1}{\chi^2}\frac{\partial C_s}{\partial t} \tag{6}$$

The first three terms are identical to Eqn. (1), while the RHS represents the dead zone source/sink term. For the dead zones,

$$\frac{\partial C_s}{\partial t} = \frac{\chi^2}{\tau}(C - C_s) \tag{7}$$

$\chi = (A/A_s)^{1/2}$ is a relative measure of the effective area of the dead zone region and τ is the characteristic time scale for the exchange of tracer particles between the bulk flow and the dead zones.

Making use of the following initial and boundary conditions,

$$C_s(x, 0) = 0 \tag{8}$$

$$C(x, 0) = \frac{M}{A}\delta(x) \tag{9}$$

$$UA\int_0^\infty C(x, t)dt = M \qquad \text{for all } x \tag{10}$$

$$As\ x \to \infty, \quad C \to 0 \tag{11}$$

where $\delta(x)$ is the Dirac delta function, the following solution

can be obtained for $C(x,t)$ via the Laplace transform method shown in Appendix A.

$$C(x,t) = \frac{M}{2A(\pi Kt)^{1/2}} \exp\left[-\frac{(x-Ut)^2}{4Kt}\right] e^{-t/\tau} + e^{-\chi^2 t/\tau} \cdot \int_0^t \frac{M}{2A(\pi Kv)^{1/2}} \exp\left[-\frac{(x-Uv)^2}{4Kv}\right] e^{\chi^2 v/\tau} \cdot \frac{\chi}{\tau} \cdot e^{-v/\tau} \cdot \left(\frac{v}{t-v}\right)^{1/2} \cdot I_1\left[\frac{2\chi}{\tau} \cdot v^{1/2} \cdot (t-v)^{1/2}\right] \cdot dv \qquad (12)$$

where v is the variable of integration and I_1 is a modified Bessel function of the first kind and first order.

The two terms of Eqn. (12) show that the tracer cloud will comprise a part obeying the simple mechanism of shear-dispersion in the bulk flow regime, described by the first term, and a part which has been affected by storage in dead zones described by the second term. As time proceeds, the exponential coefficient of the first term becomes progressively smaller, approaching zero as $t \to \infty$. This describes the declining importance of simple shear-dispersion effects as a larger and larger proportion of the particles in the tracer cloud have passed through a dead zone at least once. On the other hand, tracer which has already passed into a dead zone and then returned to the main channel will be subject to the shear-dispersion mechanism again, until it re-enters a dead zone for a further time. The first two terms after the integral sign in Eqn. (12) describe this process. They are identical to the right hand side of Eqn. (2) which is the asymptotic solution proposed by Taylor (1954) for the simple shear-dispersion process acting alone. Their reappearance in the context of the second, dead zone term of Eqn. (12) indicates the interaction of the processes in the two zones of the model channel.

If τ is infinitely large, then tracer particles will be infinitely slow in entering dead zones. In this case the last term of Eqn. (6) will be zero, $\partial C_s/\partial t$ will be zero in Eqn. (7) and Eqn. (12) will become the same as Eqn. (2). In other words, the one-dimensional ADE is a special case of the D-DZM in which tracer exchange with the dead zones takes place at a negligible rate.

The storage and release of tracer in dead zones is a powerful dispersing mechanism in itself. As a simple illustrative example, consider the case of a well mixed dead zone with an initial finite concentration at $t = 0$, i.e. $C_s(x,0) = C_0$. If there is an input of fresh water and an equivalent volume output to the bulk flow regime, then a trivial solution to Eqn. (7), which describes both the concentration within the dead zone and the output from it at time t, is given by,

$$C_s(t) = C_0 e^{-\chi^2 t/\tau} \qquad (13)$$

This exponential decay, which appears in front of the integral of the second term of Eqn. (12), expresses the effects of progressive dilution in the dead zone as tracer particles are released to the bulk flow after storage.

CALIBRATION

Calibration of the D-DZM involves identifying values of the unknown parameters K, χ and τ such that the best fit is obtained between Eqn. (12) and a particular set of field data. This was achieved by minimizing the least squares estimator,

$$F(\boldsymbol{\alpha}) = \frac{\sum_{i=1}^{n} (C_{fi} - C(\boldsymbol{\alpha})_i)^2}{\sum_{i=1}^{n} C_{fi}^2} \qquad (14)$$

in which $\boldsymbol{\alpha}$ is the parameter set $[K, \chi, \tau]$, C_f is the measured concentration, $C(\boldsymbol{\alpha})$ is the predicted cross-sectional average concentration from the model and $i = 1, n$ corresponds to n sampling times at a sampling station at x. The minimum was found using a deterministic gradient-searching algorithm developed by the Numerical Algorithms Group (NAG Library, 1990) and varying the values of K, χ and τ. The D-DZM also includes the parameters U, A and M, but these were treated as known constants with appropriate values from Atkinson and Davis (2000).

SENSITIVITY ANALYSIS

The optimization procedure tells us little about the internal form or structure of $F(\boldsymbol{\alpha})$. It is useful to know something of its sensitivity to changes in the parameters in the neighbourhood of an optimal solution $\boldsymbol{\alpha}_o$. The essential point is that redundant parameters show low sensitivity, i.e. their values can be changed considerably without significant deterioration in the fit of the model to the data (Beck, 1987). Since in the D-DZM each parameter is associated with just one physical process, sensitivity analysis should allow us to discriminate the relative importance of dead zones and shear flow dispersion. To gain insight into the nature of $F(\boldsymbol{\alpha})$ specific isovalue contours of $F(\boldsymbol{\alpha})$ about $\boldsymbol{\alpha}_0$ were examined using two separate criteria; firstly, the isovalue contour $F(\boldsymbol{\alpha}) = 1.1\ F(\boldsymbol{\alpha}_o)$, which provides the ranges in the parameters for solutions which fall within a 10% relaxation of $F(\boldsymbol{\alpha}_o)$ and secondly, the isovalue contour $F(\boldsymbol{\alpha}) = 0.09$, which was chosen as a subjective limit to the solutions of the D-DZM with an acceptable fit on a purely visual basis.

The optimal solutions of the D-DZM presented below reflect differing degrees of 'goodness of fit' so that both sensitivity criteria contain an element dependent on the value of $F(\boldsymbol{\alpha}_o)$ for that station. Since the effect of 'goodness of fit' acts proportionally and inverse-proportionally on the apparent sensitivities for $F(\boldsymbol{\alpha}) = 1.1\ F(\boldsymbol{\alpha}_o)$ and $F(\boldsymbol{\alpha}) = 0.09$ respectively, a geometric mean of the ranges in the parameters for the two criteria was calculated. This achieves a crude cancellation of the effect of differing values of $F(\boldsymbol{\alpha}_o)$ upon the apparent sensitivities. The combined sensitivity

index therefore shows the range within which each parameter can be changed without producing a noticeable degradation of the fit of Eqn. (12) to the shape of the tracer cloud as recorded at each station.

Application of the D-DZM to the River Severn

The optimal fits for parameters K, χ and τ for each station are given in Table 2 and compared with the data in Fig. 5. Clearly, with a reach-by-reach variation in the model parameters, the D-DZM can describe individual tracer curves quite well. The values of $F(\alpha_o)$ are low and the solutions are visually acceptable at most stations.

It is comparatively easy for a dispersion model to describe individual tracer distributions. A much more important test for the D-DZM is that any successful model should be able to describe the evolution of the dispersing cloud with physically realistic downstream trends in the parameters. For a channel with nearly uniform flow properties or statistically nearly uniform geometry, "physically realistic" is likely to mean no trend at all, i.e. constant or nearly constant parameter values. Clearly the dispersion coefficient K depends upon the transverse velocity distribution over the bulk flow. If this has no downstream trend, as it should not in a channel with no downstream trend in velocity and

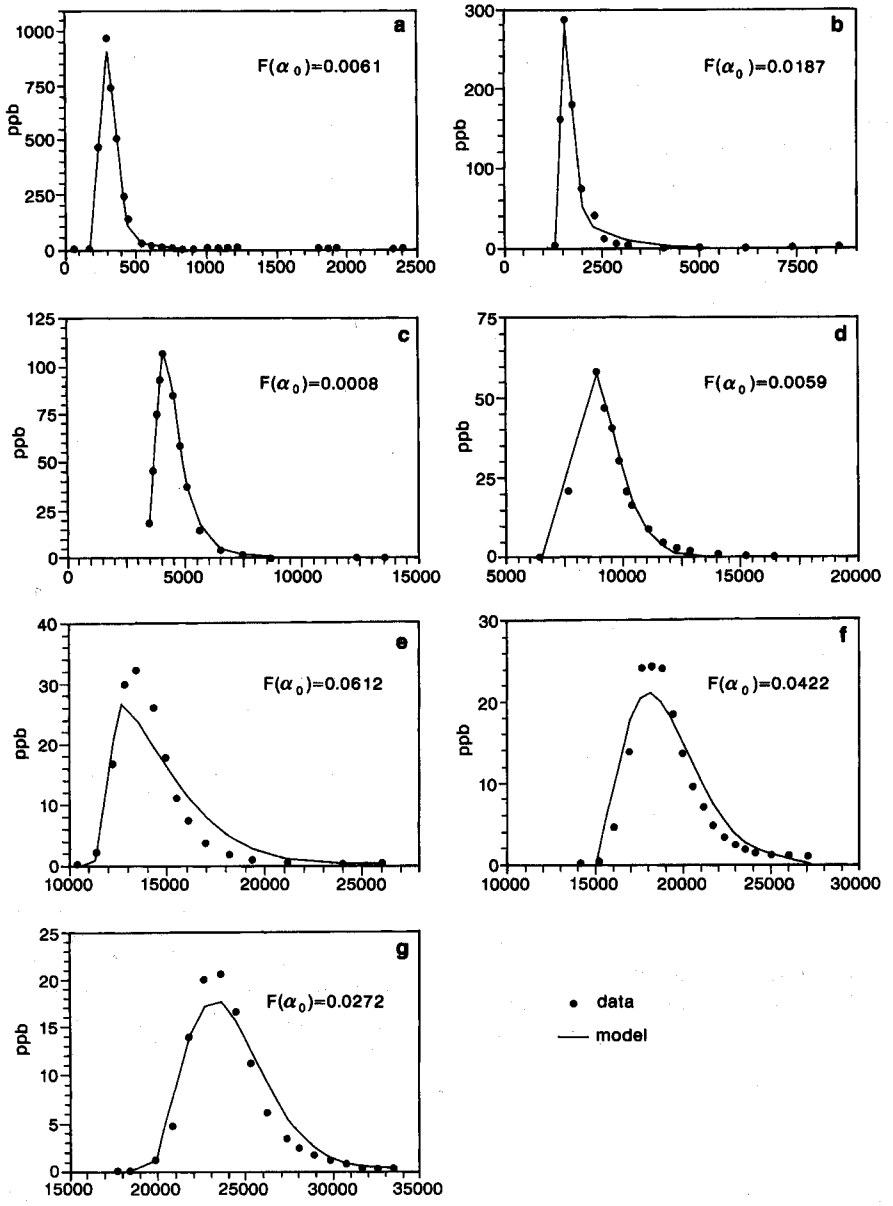

Fig. 5. *Empirical tracer distributions (closed circles) and optimal solutions α_o of the D-DZM (unbroken line) with corresponding values of $F(\alpha_o)$ for stations A to G.*

only a very weak trend in width, then only very weak trends in K may be expected. In the general case, χ and τ probably depend on the channel shape and the geometry of the dead zones, so they could be functions of longitudinal distance. In the case of the River Severn, however, the irregularity of the channel, as expressed by the variance of its dimensions, shows little downstream trend. So it is reasonable to expect χ to be nearly constant along the whole test reach. The timescale parameter τ depends on both the dead zone geometry and on the speed of exchange between dead zones and the bulk flow. Once again, there is little reason to expect a systematic change in parameters along the reach, although this expectation is somewhat less certain than for χ and K.

In the D-DZM the whole reach length from $x = 0$ is treated as a single dead zone element. Because of this, parameter values established by best-fit at a particular station include the effects of the whole channel upstream. Therefore, two criteria must be satisfied if the model is to be regarded as providing a satisfactory description of the cloud's evolution. Firstly, the fitted values should display little or no overall downstream trend, in accordance with the expectations derived from near-constancy of velocity and geometry. Secondly, the sensitivity ranges of parameters should overlap (or since sensitivity range is defined partly subjectively, they should almost overlap). This implies that a set $\boldsymbol{\alpha}$ consisting of a single value for each parameter could be chosen which would give a satisfactory simulation of the data at *all* stations, thus describing the whole observed evolution of the cloud.

CONSTANT PARAMETER PREDICTION

The results of the sensitivity analysis for K, χ and τ are shown in Figs. 6a, 6b, 6c respectively. The figures show the geometric mean of the ranges in the sensitivity of the parameters and also the optimal solutions from Table 2.

Stations A, B and C show a significant trend in the longitudinal shear-dispersion coefficient K (Fig. 6a). This is to be expected as it has already been shown that mixing over the bulk flow region becomes established by the time station C is reached. To assess the predictive ability of the D-DZM, the values of K at stations A and B are therefore ignored. There is a good physical argument for setting the shear-dispersion coefficient for the whole reach to a constant value given by K for station C. Because mixing over the bulk flow regime has been established in the reach between B and C, K at station C defines shear-dispersion over the whole of the bulk flow regime. Any tracer particles that have already migrated into dead zone regions upstream of C are accounted for by the dead zone storage term and not in the best-fit value of K. (This is not the case for the value of K_c at station C (Table 1), which implicitly incorporates the diluting effect of tracer storage, and is 10% larger than K derived from fitting the D-DZM as a result).

By the criteria given above for a successful model,

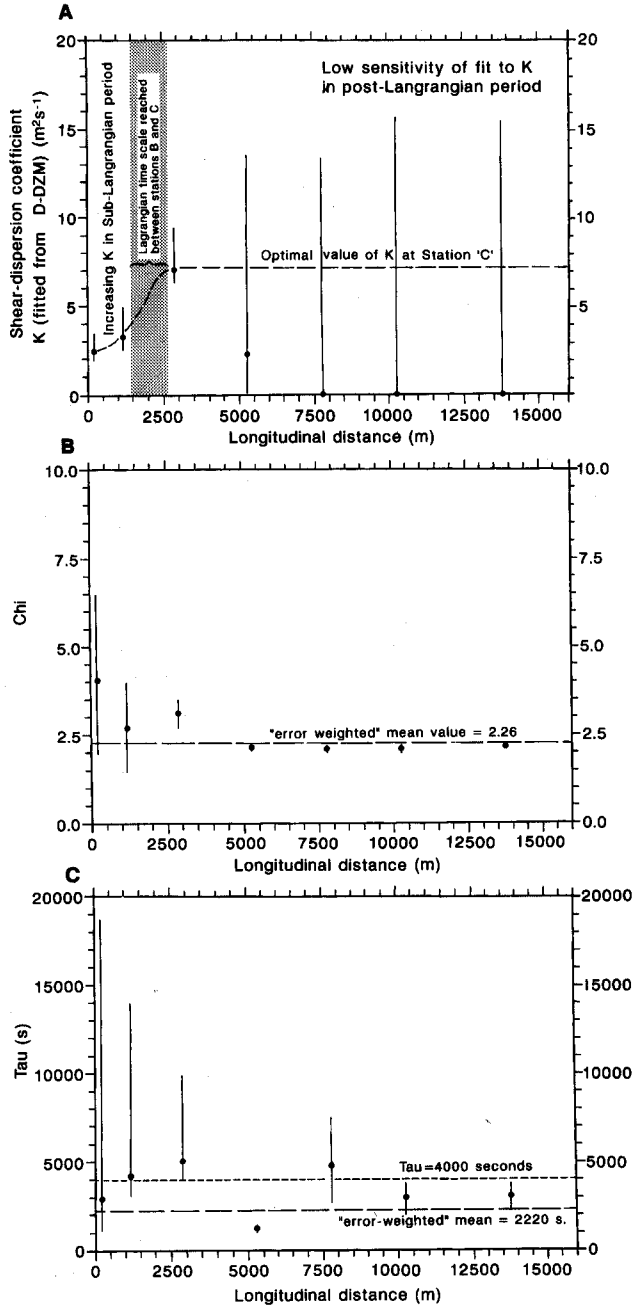

Fig. 6. *(a) Geometric mean of sensitivity of* $F(\alpha_o)$ *to K about optimal solutions of the D-DZM (vertical lines) versus longitudinal distance. The optimal solutions of K are shown as closed dots. (b) Geometric mean of sensitivity of* $F(\alpha_o)$ *to* χ *about optimal solutions of the D-DZM (vertical lines) versus longitudinal distance. The optimal solutions of* χ *are shown as closed dots. (c) Geometric mean of sensitivity of* $F(\alpha_o)$ *to* τ *about optimal solutions of the D-DZM (vertical lines) versus longitudinal distance. The optimal solutions of* τ *are shown as closed dots.*

stations D, E, F and G should possess the same value of K as station C. The best-fit values are in fact very different from the value at station C, but the marked insensitivity to K shown by the vertical bars for each point in Fig. 6a indicates

that similarly good fits could be obtained for large ranges in K which overlap the value at C. Thus, although there is a downstream trend of reducing best-fit values of K this cannot be regarded as significant, since the value from the initial station in the trend, C, would give almost as good a result as the optimum fits. In the case of K, therefore, the D-DZM satisfies the second criterion of success in describing the evolution of the tracer cloud, but not the first. To the extent that the second criterion subsumes the first (i.e. the trend is not "significant" in sensitivity terms), the fitted values of K in the D-DZM may be regarded as satisfying the expectations of constancy posited on the basis of near-constant velocity and channel geometry. The only *significant* trend in fitted values of K is in the first three stations, and this is readily explainable in terms of mixing during the pre-Lagrangian period established from Fig. 2.

Figure 6b shows the optimal solutions and the range in sensitivities for χ. There is a certain amount of scatter among the early stations, but this can be explained partly by insensitivity to changes in the value of χ. The average value of χ for the last four stations (D through G) lies within the sensitivity ranges of stations A and B. Stations D through G are particularly well-behaved with regard to χ, which is clearly constant over this part of the study reach. Thus, in the downstream part of the reach, the D-DZM clearly meets both the criteria for success in describing the cloud's evolution. However, the tendency towards higher values of χ in the upstream part requires explanation. The data show that over the pre-Lagrangian time period the values of χ are higher than further downstream. Thus, the ratio A/A_s is larger and the dead zones appear to have a smaller effective size in the upstream part. This might be expected if mixing in the bulk flow regime were incomplete. A greater-than-average proportion of the tracer would be concentrated near the centre of the channel from which dead zones in the banks would be inaccessible. The D-DZM, on the other hand, is based on an assumption of complete mixing which applies only in the post-Lagrangian period. This provides a physical explanation for the higher values of χ and the apparently smaller dead zones at the first three stations. It also explains why the sensitivity range of χ decreases from A to C. At A and B, little of the tracer will have passed through a dead zone, so that the solution is not sensitive to χ. By the time the cloud reaches station C, a significant proportion of tracer particles have passed through a dead zone, and so the sensitivity to this parameter is enhanced.

For predictive purposes a constant value of χ can be chosen by $\sum_{j=1}^{7} \chi_{0j} w_j / \sum_{j=1}^{7} w_j = 2.26$, where w is the inverse of the range of the geometric mean in Fig. 6b. On this basis, the effective cross-sectional area of the dead zone storage region A_s is approximately 2 m^2 which from general field observations seems a realistic value for backwaters created by the pool-riffle sequence, bank irregularities, and slack water in the cores of meanders.

The optimal solutions of τ (Fig. 6c) show no significant trend downstream. However they do show a larger degree of scatter, relative to sensitivity ranges, than either χ or K. A value of $\tau = 4000$ seconds gives a near-overlap to the sensitivity ranges of all stations except D. The "error-weighted" mean value of τ is 2220 seconds, calculated as for χ above. The parameter τ governs the ratio of the first and second terms of Eqn. (12) according to the exponent $e^{-t/\tau}$ in the first term and is a characteristic time scale for the exchange of tracer particles between the bulk flow regime and dead zone storage region. At $t = \tau$, 63% of the tracer particles have passed through the dead zone storage mechanism at least once. For $t = 2\tau$ and $t = 3\tau$ the proportions are 87% and 95% respectively. Values of τ within the range 1200 to 5100 seconds demonstrate that the exchange of tracer with the dead zone system takes place on a timescale of twenty minutes or more in the River Severn. This is much longer than the lifetime of individual turbulent eddies. The time-scale for shear flow dispersion within the channel can be estimated from L^2/K where L is a characteristic channel dimension (e.g. $L\sim$ average width $\approx$24 m, or $L^2\sim$ average cross-sectional area $\approx$12 m^2). With $K \approx 7\ m^2 s^{-1}$ this timescale lies in the range 2–80 s, which is one to three orders of magnitude smaller than τ. Therefore, a slower mechanism than simple eddy diffusion must transport tracer into and out of dead zones. One group of probable candidates are occasional larger-than-average eddies which enter the mouths of backwaters and embayments in the bank, or swirl into the slower moving parts of pools. From observation, these eddies occur every few minutes and are capable of a temporary but vigorous displacement of slow-moving or static water. This comparison militates in favour of identifying the D-DZM's dead zones with backwaters and embayments which are an ubiquitous feature of the River Severn's channel. It does not preclude other possibilities, however, such as molecular diffusion into the pores between the gravel particles on the bed. But an effective dead zone area of $\sim$2 m^2 would require physical penetration of tracer for some 0.3–0.5 m into the gravel, depending on the porosity. Since the interstices are invariably packed with smaller stones and sand beneath the top layer of particles, this seems very unlikely. The value of τ, therefore, suggests that backwaters and embayments are the most likely physical features to be acting as dead zones. A residence timescale for tracer particles in the dead zone storage system is given by τ/χ^2. For the range of values of τ, this suggests that tracer particles will spend, on average, between 230 s and 1000 s in storage before returning to the bulk flow regime. Visual observation of tracer at the time of the dispersion test indicated residence times of this order in eddies and backwaters, which tends to confirm the argument that these features are the main ones acting as dead zones.

It is, nevertheless, difficult to identify an optimum value for τ which might be taken to apply to the whole length of the channel. Because there is no trend in values, any one of three estimates might apply, i.e. the simple mean (3470 s), "error-weighted" mean (2220 s) or "nearest overlap"

(4000 s). As Beck (1987) stated; "to fix the most uncertain parameter seems a logical contradiction. It implies perfect knowledge of the least certain parameter." Thus, a fourth alternative for predictive purposes is to allow τ to vary from station to station, assuming its optimal value (Table 2) at each.

Within certain bounds therefore, the D-DZM does predict approximately constant parameters as was suggested by the characteristics of the flow and channel. It is now possible to ascertain whether the model is able to predict the statistical properties of the evolving cloud with constant parameters $K = 7.16\ m^2s^{-1}$ and $\chi = 2.26$, with $\tau = \tau_{optimum}$. The results are shown in Fig. 7 with the appropriate values of $F(\alpha)$. With the exception of station A and B, constant-parameter model provides acceptable fits. Peak heights are correct to within 10–15%, peak timing shows excellent agreement and "tailing" or asymmetry is represented satisfactorily or well. In the downstream stations, there is a tendency for the modelled concentrations to rise too steeply initially, but this discrepancy is not serious. Much poorer fits are to be expected at stations A and B, as the tracer there appears not to have mixed fully over the bulk flow region. In addition, the chosen value of $\chi = 2.26$ is heavily weighted toward the optimal values at stations D through G because of the greater sensitivity of $F(\alpha)$ to changes in χ there. This explains the inadequacy of the

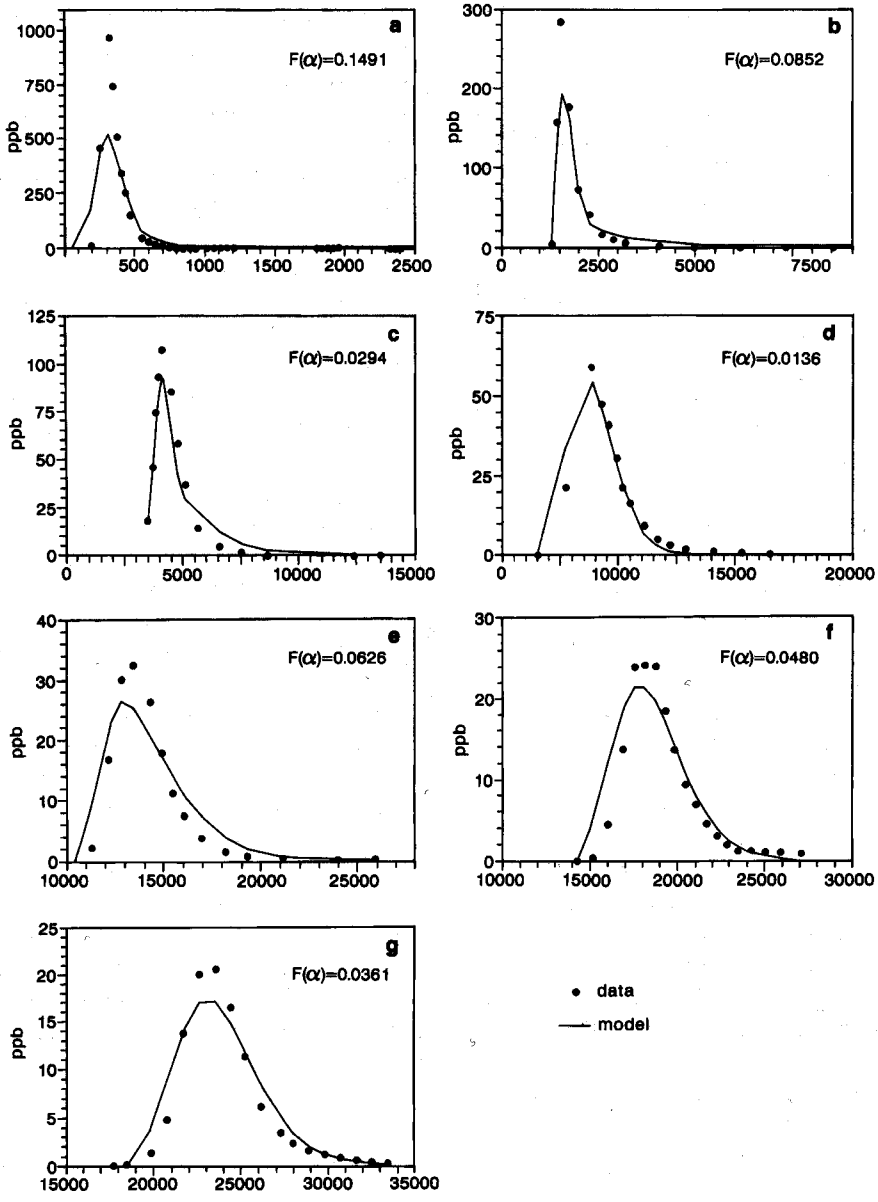

Fig. 7. *Empirical tracer distributions (closed circles) and the D-DZM (line) with constant parameters, $K = 7.16\ m^2s^{-1}$ and $\chi = 2.26$ with $\tau = \tau_o$, and corresponding values of* $F(\alpha)$ *for stations A to G.*

model with respect to the general shape of the cloud at A and the peak height at B where tailing is well represented (Fig. 7).

The predictive abilities of the D-DZM to describe downstream trends in peak concentration and the temporal variance of the tracer distributions are shown in Fig. 8, which may be compared with the performance of the one-dimensional ADE shown in Fig. 4. Clearly, after cross-sectional mixing is established over the bulk flow, the model is a vast improvement on simple shear-dispersion. Figure 8a demonstrates that the dead zone storage process can account for the non-Fickian rate of peak attenuation. Figure 8b shows that it also accounts for the magnitude and growth rate of temporal variance.

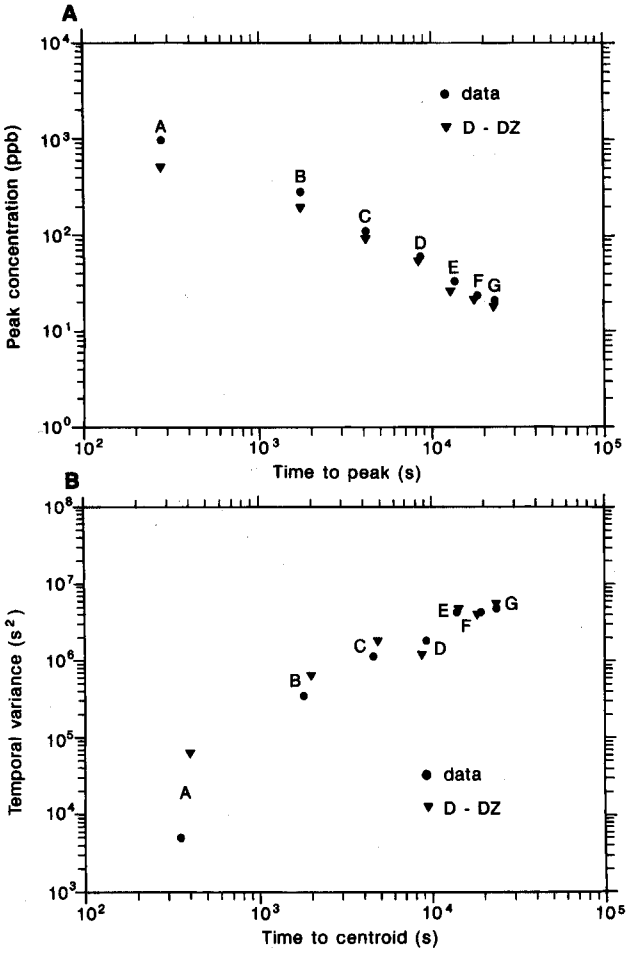

Fig. 8. *(a) Decay with distance of the peak cloud concentration (closed circles) compared with that predicted by the D-DZM with the constant parameters* $K = 7.16\ m^2 s^{-1}$ *and* $\chi = 2.26$ *with* $\tau = \tau_o$ *(closed triangles). (b) Temporal variance,* σ_τ^2 *of the tracer cloud (closed circles) compared with predictions by the SFD-DZM with the constant parameters* $K = 7.16\ m^2 s^{-1}$ *and* $\chi = 2.26$ *with* $\tau = \tau_o$ *(closed triangles).*

RELATIVE IMPORTANCE OF DISPERSION MECHANISMS

Sensitivity analysis is useful as a tool for hypothesis discrimination. When the objective function $F(\alpha)$ is insensitive to a parameter, the dispersing mechanism that it describes is relatively unimportant at that particular station since there are a wide range of parameter values giving almost equally "good" fits of the model to the data.

From the results of the sensitivity analysis, it is possible to identify two periods in the tracer cloud's evolution when either shear-dispersion or the dead zone mechanism is dominant. Between these two end members, there is a transition in which neither dominates but both act together.

The Pre-Lagrangian Time Period

Figure 5 shows that the D-DZM is capable of describing the tracer distributions at stations A and B provided that the optimal solutions are used. These are sensitive to the value of K (Fig. 6a), but are much less sensitive to changes in χ and τ (Figs. 6b and 6c), which suggests that shear-dispersion is the dominant process. The first and second terms of Eqn. (12) are plotted separately for the optimal solutions at stations A and B in Fig. 9. The dominance of the first term shows that a large proportion of tracer particles have not yet entered dead zones for the first time. Thus, dead zones are a much less important mechanism than simple shear-flow dispersion at this early stage in the cloud's evolution. Nevertheless, dead zones still need to be invoked in order to account for the definite tailing of the tracer curves, which Fig. 1 shows is greater than expected from the ADE model Eqn. 2.

The Lagrangian time and distance scales for mixing over the bulk flow were identified above, using the criterion that the ratio $U_c/\overline{u}_s$ should be equal to unity and an implicit assumption that dead zones have no important effects on the leading edge of the cloud while initial cross-sectional mixing is established. Figure 9 confirms this assumption. At stations A and B, only a very small proportion of the tracer particles that constitute the leading edges of the optimal solutions (i.e., for $t < 250$ s and $t < 1600$ s respectively) appear on the basis of the model to have passed through dead zones.

The Post-Lagrangian Time Period

Figure 6 shows that in the post-Lagrangian period only station C is sensitive to all three parameters K, χ and τ. This is also the point at which the D-DZM is particularly accurate (see Figs. 5 and 7). Figure 9c shows the first and second terms of Eqn. (12) for station C. It is clear that roughly half of the tracer has passed through dead zones at least once. Thus, neither shear-dispersion nor the dead zone mechanism is dominant at Station C but both act together.

For stations D, E, F and G the model fits are not at all sensitive to the value of K. This suggests that the dispersion process is dominated by the dead zone mechanism, which is

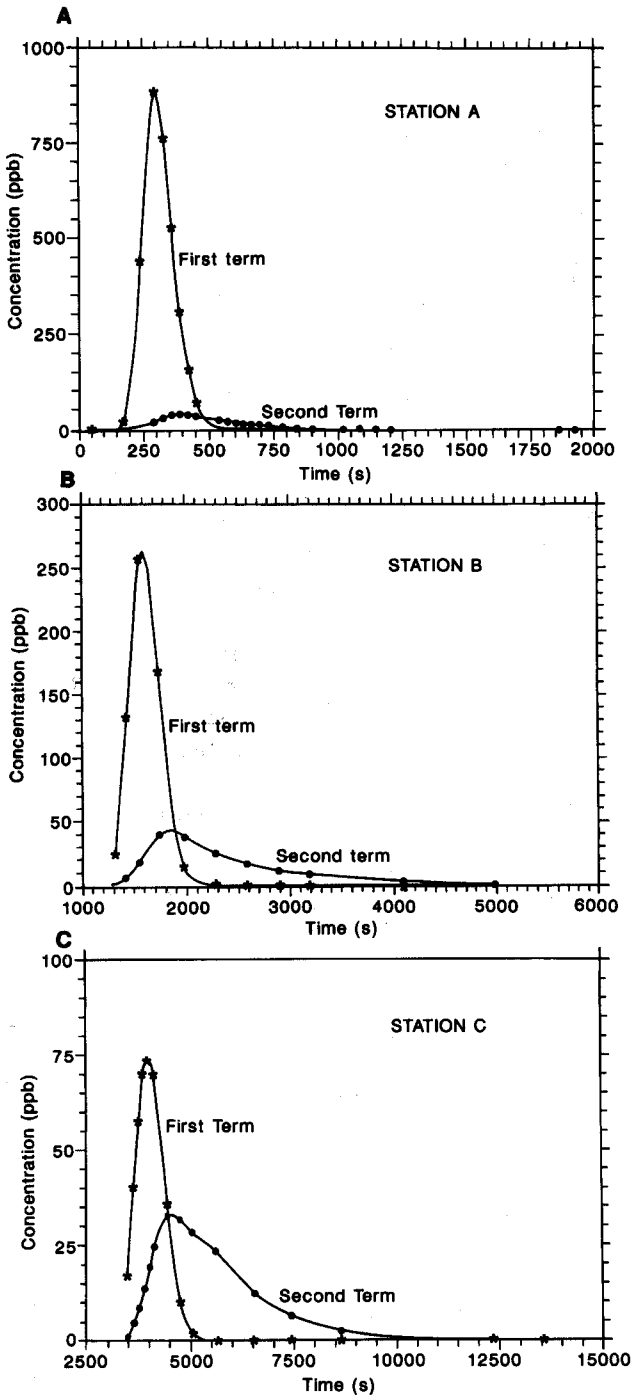

Fig. 9. *(a) First and second terms of Eq. (12) with optimal solution* α_o *for station A. (b) First and second terms of Eq. (12) with optimal solution* α_o *for station B. (c) First and second terms of Eq. (12) with the constant parameters* $K = 7.16\ m^2s^{-1}$ *and* $\chi = 2.26$ *with* $\tau = \tau_o$ *for station C.*

confirmed by high sensitivity to χ and τ (Fig. 6). The percentage of the mass in the first term of Eqn. (12) for stations D, E, F and G (with $K = 7.16\ m^2s^{-1}$, $\chi = 2.26$ and $\tau = \tau_{optimum}$) are 0.01%, 6.88%, 0.28% and 0.04% respectively. This indicates that all but a very small proportion of tracer particles have passed through dead zones at least once. This confirms the suggestion made above that the slowing of the cloud velocity relative to the water in the bulk flow region (Fig. 2) is due to storage of tracer from the leading edge of the cloud in dead zones.

Quasi-Gaussian leading edges are a persistent feature of empirical data from natural channels. The shear-dispersion process is responsible for their formation in the pre-Lagrangian time period (stations A and B) and in early post-Lagrangian time (station C). At longer times (corresponding to stations D through to G) the leading edges of the cloud are diluted by dead zone storage, yet their Gaussian appearance is preserved (see Fig. 1 in which straight lines can be fitted to the leading edge parts of the data on a Chatwin plot). Quasi-Gaussian leading edges are observed so often in empirical data that they are often thought to signify the importance of shear-dispersion effects. This is not strictly the case. The values of K_c determined by Chatwin's analysis (Table 1) describe the pseudo-Gaussian form, combining in one coefficient the dispersive effects of shear-flow and the more important effects of dead zone storage.

At stations D, E, F and G the first term of the D-DZM is unimportant. Although shear-flow dispersion still occurs, as reflected by the coefficient K's occurrence within the integral of the second term of Eqn. (12), it is relatively unimportant in comparison with the dead zone process. Not only is there a large range of almost equally suitable solutions for K at each station, but the optimal values (Table 2) tend towards zero. This is strong evidence for the contention of Beer and Young (1983) and Wallis *et al.* (1989) that dispersion is dominated by the dead zone mechanism once full mixing has been established over the channel cross-section. It suggests that the cloud shapes at stations D-G could perhaps be predicted realistically by a model incorporating dead zone storage alone, without any consideration of the shear-dispersion in the bulk flow region. This idea is developed further in a companion paper (Davis and Atkinson, 2000).

Conclusions

Once full mixing of tracer over the bulk flow has been established, the two mechanisms of shear flow dispersion and dead zones both contribute to longitudinal dispersion. The D-DZM models the decline of peak concentration, growth of variance, and overall cloud shape successfully while keeping parameter values constant or within a narrow range. Thus, dead zone storage accounts for the non-Fickian elements in the tracer cloud's evolution. Furthermore, sensitivity analysis and comparison of first and second terms in the D-DZM demonstrate the relative importance of the two mechanisms. There are two distinct stages of cloud evolution with a rapid transitional phase between them. In the time period before mixing over the whole bulk

flow regime is established, corresponding to stations A and B, the dispersion process is characterised by values of $t/\tau \ll 1$ and $U_c/\bar{u}_s > 1$, indicating that little of the tracer has passed through dead zone storage and that the tracer particles have not yet fully sampled the range of velocities found in the bulk flow region. The shear-dispersion mechanism dominates, although the limiting one-dimensional model of Eqns. (1) and (2) does not apply. The most appropriate mathematical model for this time period would involve a two-dimensional treatment with local values of turbulent dispersion coefficient (*e.g.* Smith, 1982; Chatwin and Allen, 1985).

For a short transitional period just after mixing over the bulk flow region is established, when the value of $t/\tau \sim 1$ (corresponding to station C), about 50% of the tracer particles have passed through the dead zone storage mechanism at least once. Tracer particles near the peak of the cloud have an average velocity very nearly equal to the discharge velocity. In this transitional stage, a rough equality of terms from Eqn. (6) holds, such that $\chi^2(C - C_s)/\tau \approx K(\partial^2 C/\partial x^2)$.

The second distinct stage of cloud evolution corresponds to stations D–G, where $t/\tau > 3$ and comparison of terms indicates that more than 95% of the tracer particles have passed through the dead zone storage mechanism at least once. Thus, $\chi^2(C - C_s)/\tau \rangle\rangle K(\partial^2 C/\partial x^2)$, demonstrating the dominant contribution that the accumulated effects of dead zone storage have made to the overall dispersion process. As a result, tracer particles in the leading part of the cloud in the River Severn have an average velocity of approximately 85% of the discharge velocity.

Acknowledgements

John Barker made valuable suggestions for improvements to an earlier version of this paper. P.M. Davis was supported by a Natural Environment Research Council Training Award.

List of Symbols

A	cross-sectional area of the bulk flow region of a channel
A_S	cross-sectional area of dead zone region of a channel
A^*	Chatwin parameter, $M/(2A(\pi K)^{1/2})$
C	cross-sectionally averaged concentration of tracer
C_f	tracer concentration measured in field data
C_p	peak concentration of tracer
C_s	tracer concentration in dead zone
$C_T(x,t)$	concentration as defined by the Advection-Dispersion Equation
K	longitudinal dispersion coefficient in the bulk flow region
K_c	estimated value of K based on Chatwin's analysis of the rising limb and peak of a tracer curve
M	Mass of tracer injected
t	time elapsed since tracer injection
$\bar{t}$	time from injection to centroid of tracer distribution
U	average streamwise velocity in the bulk flow region
U_c	estimated value of U based on Chatwin's analysis of the rising limb and peak of a tracer curve
$\bar{u}_s$	average water velocity upstream of a station s
w_j	weighting factor for parameter averaging, based on sensitivity range of the parameter at the jth station
x	streamwise distance from point of tracer injection
$\boldsymbol{\alpha}$	the parameter set $[K, \chi, \tau]$
$\boldsymbol{\alpha}_o$	best-fit parameter set $[K_o, \chi_o, \tau_o]$
$\delta(x)$	Dirac delta function of x
α, β, θ, s	symbols used and defined in Appendix One
ν	variable of integration
σ_t^2	temporal variance of tracer distribution
σ_x^2	spatial variance of tracer distribution
τ	characteristic time sacle of tracer exchange between mobile and stationary regions of the channel
χ	dead zone storage parameter, defined by $\chi^2 = A/A_s$

References

Aris, R., 1959. The longitudinal diffusion coefficient in flow through a tube with stagnant pockets. *Chem. Eng. Sci.*, 11, 194–198.

Atkinson, T.C. and Davis, P.M., 2000. Longitudinal dispersion in natural channels: 1. Experimental results from the River Severn, Britain. *Hydrol. Earth System Sci.*, **4**, 345–353.

Barker, J.A., 1982. Laplace transform solutions for solute transport in fissured aquifers. *Adv. Water Resources*, **5**, 98–104.

Beck, M.B., 1987. Water quality modeling: a review of the analysis of uncertainty. *Water Resour. Res.*, **23**, 1393–1442.

Beer, T. and Young, P.C., 1983. Longitudinal dispersion in natural streams. *J. Environ. Eng. A.S.C.E.*, **109**, 1049–1067.

Bencala, K.F. and Walters, R.A., 1983. Simulation of solute transport in a mountain pool-and-riffle system: A transient storage model. *Water Resour. Res.*, **19**, 718–724.

Carnahan, C.L. and Remer, J.S., 1984. Nonequilibrium and equilibrium sorption with linear sorption isotherm during transport through an infinite porous medium: some analytical solutions. *J. Hydrol.*, **73**, 227–258.

Chatwin, P.C., 1971. On the interpretation of some longitudinal dispersion experiments. *J. Fluid Mech.*, **48**, 689–702.

Chatwin, P.C., 1973. A calculation illustrating effects of the viscous sublayer on longitudinal dispersion. *Quart. J. Mech. Appl. Math.*, **26**, 427–439.

Coats, N.H. and Smith, B.D., 1964. Dead end pore volume and dispersion in porous media. *Soc. Petrol. Engrs. J.*, **4**, 73–84.

Day, T.J., 1975. Longitudinal dispersion in natural channels. *Water Resour. Res.*, **11**, 909–918.

Day, T.J. and Wood, I.R., 1976. Similarity of the mean motion of fluid particles dispersing in a natural channel. *Water Resour. Res.*, **12**, 655–666.

Davis, P.M. and Atkinson, T.C., 2000. Longitudinal dispersion in natural channels: 3. An aggregated dead zone model and its

application to the River Severn, Britain. *Hydrol. Earth System Sci.*, **4**, 373–381.
Denton, R.A., 1990. Analytical asymptotic solution for longitudinal dispersion with dead zones. *J. Hydraul. Res.*, **28**, 309–329.
De Smedt, F. and Wieringa, P.J., 1979a. A generalised solution for solute flow in soils with mobile and immobile water. *Water Resour. Res.*, **15**, 1137–1141.
De Smedt, F. and Wieringa, P.J., 1979b. Mass transfer in porous media with immobile water. *J. Hydrol.*, **41**, 59–67.
Dewey, R. and Sullivan, P.J., 1977. The asymptotic stage of longitudinal turbulent dispersion within a tube. *J. Fluid Mech.*, **80**, 293–303.
Elder, J.W., 1959. The dispersion of marked fluid in turbulent shear flow. *J. Fluid Mech.*, **5**, 544–560.
Fischer, H.B., 1966. Longitudinal dispersion in laboratory and natural streams. *Technical Report ~ KH-R-12*, W.M. Keck Laboratory of Hydraulics and Water Resources.
Fischer, H.B., 1967. The mechanics of dispersion in natural streams. *J. Hydraul. Div. A.S.C.E.*, **93**, 187–216.
Fischer, H.B., 1968. Methods for predicting dispersion coefficients in natural streams, with applications to lower reaches of the Green and Duwamish Rivers, *U.S. Geol. Surv. Prof. Pap.*, **582(A)**.
Godfrey, R.G. and Frederick, B.J., 1970. Stream dispersion at selected sites. *U.S. Geol. Surv. Prof. Pap.*, **433(K)**.
Hays, J.R., 1966. *Mass transport mechanisms in open channel flow.* Ph.D. thesis, Vanderbilt Univ., Tennessee.
Hays, J.R. and Krenkel, P.A., 1968. Mathematical modeling of mixing phenomena in rivers. *University of Texas Water Resources Symposium*, **1**, 111–123.
Lapidus, L. and Amundson, N.R., 1952. Mathematics of adsorption in beds. VI The effect of longitudinal dispersion in ion exchange and chromatographic columns. *J. Phys. Chem.*, **56**, 984–988.
Legrand-Marcq, C. and Laudelout, H., 1985. Longitudinal dispersion in a forest stream. *J. Hydrol.*, **78**, 317–324.
Moench, A.F., 1989. Convergent radial dispersion: a Laplace transform solution for aquifer tracer testing. *Water Resour. Res.*, **25**, 439–447.
Moench, A.F., 1991. Convergent radial dispersion: a note on evaluation of the Laplace transform solution. *Water Resour. Res.*, **27**, 3261–3264.
NAG Library, 1990. *Mark 14, subroutine E04JAF, Rep. 1435/0:Mk6:77.* Numerical Algorithms Group, Oxford.
Nordin, C.F. and Sabol, G.V., 1974. Empirical data on longitudinal dispersion in rivers. *U.S. Geol. Surv. Water Resour. Invest.*, 20–74.
Nordin, C.F. and Troutman, B.M., 1980. Longitudinal dispersion in rivers: the persistence of skewness in observed data. *Water Resour. Res.*, **16**, 123–128.
Patterson, C.C., 1968. A discussion of "Mathematical modelling of mixing phenomena in rivers" by Hays and Krenkel (1968). *University of Texas Water Resources Symposium*, **1**, 124–125.
Purnama, A., 1988a. The effect of dead zones on longitudinal dispersion in streams. *J. Fluid Mech.*, **186**, 351–377.
Purnama, A., 1988b. Boundary retention effects upon contaminant dispersion in parallel flows. *J. Fluid Mech.*, **195**, 393–412.
Roberts, G.E. and Kaufmann, H., 1966. *Table of Laplace Transforms.* W.B. Saunders Company, Philadelphia and London, 367 pp.
Rutherford, J.C., Taylor, M.E.U. and Davies, J.D. 1980. Waikato River pollutant flushing rates. *J. Environ. Eng. A.S.C.E.*, **106**, 1131–1150.
Sayre, W.W. and Chang, F.M. 1968. A laboratory investigation of open-channel dispersion processes for dissolved, suspended, and floating dispersants. *U.S. Geol. Surv. Prof. Pap.*, **433(E)**.
Schnelle, K.B., Thackston, E.L. and Krenkel, P.A., 1967. Mathematical modelling of dispersion in rivers. *Proc. 12th Congress, Int. Assoc. Hydraul. Res.*, **4**, 33–41.
Sullivan, P.J., 1971. Longitudinal dispersion within a 2-D turbulent shear flow *J. Fluid Mech.*, **49**, 551–576.
Taylor, G.I., 1921. Diffusion by continuous movement. *Proc. London Math. Soc., Series 2*, **20**, 196–212.
Taylor, G.I., 1954. The dispersion of matter in turbulent flow through a pipe *Proc. Roy. Soc. London, Ser. A*, **223**, 446–468.
Thackston, E.C. and Schnelle, K.B., 1970. Predicting effects of dead zones on stream mixing. *J. Sanit. Eng. Div. A.S.C.E.*, **96**, 319–331.
Valentine, E.M. and Wood, I.R., 1977. Longitudinal dispersion with dead zones *J. Hydraul. Div. A.S.C.E.*, **103**, 975–990.
Valentine, E.M. and Wood, I.R., 1979a. Experiments in longitudinal dispersion with dead zones. *J. Hydraul. Div. A.S.C.E.*, **105**, 999–1016.
Valentine, E.M. and Wood, I.R., 1979b. Dispersion in rough rectangular channels. *J. Hydraul. Div. A.S.C.E.*, **105**, 1537–1553.
Villermaux, J. and Van Swaaij, W.P.M., 1969. Modèle representatif de la distribution des temps de séjour dans un réacteur semi-infini à dispersion axiale avec zones stagnantes. Application à l'écoulement ruisselant dans des colonnes d'anneaux Raschig. *Chem. Engng. Sci.*, **24**, 1097–1111.
Wallis, S.G., Young, P.C. and Beven, K.J., 1989. Experimental investigation of the aggregated dead zone model for longitudinal solute transport in stream channels. *Proc. Inst. Civ. Engrs, Part 2.*, **87**, 1–22.
Yotsukura, N., Fischer, H.B. and Sayre, W.W., 1970. Measurement of mixing characteristics of the Missouri River between Sioux City, Iowa, and Plattsmouth, Nebraska. *U.S. Geol. Surv. Water Supply Pap.*, **1899-G**.

Appendix A: analytical solution

The solution to Eqns. (6) and (7) subject to Eqns. (8), (9), (10) and (11) is derived as follows. Making use of the Laplace transform method;

$$\tilde{f}(p) = L\{f(t)\} = \int_0^\infty e^{-pt} f(t)dt,$$

which gives:

$$p\tilde{C} - C(0) + U\frac{d\tilde{C}}{dx} = K\frac{d^2\tilde{C}}{dx^2} - \frac{1}{\tau}(\tilde{C} - \tilde{C}_s) \qquad (15)$$

and

$$p\tilde{C}_s - C_s(0) = \frac{\chi^2}{\tau}(\tilde{C} - \tilde{C}_s) \qquad (16)$$

for Eqns. (6) and (7) where $\tilde{C}$ and $\tilde{C}_s$ are the Laplace transforms of C and C_s respectively, and $C(0)$ and $C_s(0)$ are the values of C and C_s at $t = 0$.

Eliminating $\tilde{C}_s$ from (15) using (16) and applying the initial condition Eqn. (8) results in the following linear inhomogeneous Eqn. with constant coefficients,

$$\frac{d^2\tilde{C}}{dx^2} - \frac{U}{K}\frac{d\tilde{C}}{dx} - \frac{\tilde{C}}{K}\left[\frac{1}{\tau} - \frac{\chi^2}{\tau(p\tau + \chi^2)} + p\right] = -\frac{C(0)}{K} \qquad (17)$$

The general solution of (17) is given by,

$$\tilde{C} = e^{ax}\left[A_* + \frac{1}{(b-a)}\int_0^x \frac{C(0)}{K}e^{-ax}dx\right] + e^{bx}\left[B_* - \frac{1}{(b-a)}\int_0^x \frac{C(0)}{K}e^{-bx}dx\right] \qquad (18)$$

where A_* and B_* are constants to be evaluated from

boundary conditions, and a and b are the roots of the auxiliary equation of the left hand side of (17).

Applying (9) we see the integral terms in (18) have the form,

$$\frac{M}{AK}\int_0^x \delta(x)e^{\gamma x}dx = \frac{M}{AK} \tag{19}$$

Therefore, (18) becomes,

$$\tilde{C} = e^{ax}\left[A_* + \frac{M}{(b-a)AK}\right] + e^{bx}\left[B_* - \frac{M}{(b-a)AK}\right] \tag{20}$$

Evaluating the roots of the auxiliary equation of the left hand side of (17):

$$a = \frac{U}{2K} - \frac{U}{2K}\left(1 + \frac{4WK}{U^2}\right)^{1/2},$$
$$b = \frac{U}{2K} + \frac{U}{2K}\left(1 + \frac{4WK}{U^2}\right)^{1/2} \tag{21}$$

where $W = [1/\tau - \chi^2/(p\tau^2 + \chi^2\tau) + p]$.

Applying (11), $[B_* - M/(b-a)AK] = 0$ in order for the second term of (20) not to be infinitely large when $x \to \infty$.

Applying (10) when $p = 0$, $\tilde{C} = M/UA$. By evaluating $(b-a)$ with $p = 0$, $A_* = 0$.

Therefore, (18) is reduced to

$$\tilde{C} = \frac{M}{(b-a)AK}e^{ax} \tag{22}$$

To obtain the solution in explicit form, the inverse Laplace transform of (22) must be determined. Substituting a and b from (21) into (22) we can obtain,

$$\tilde{C} = \frac{M}{2AK^{1/2}}e^{Ux/2K}\left(\frac{q^2+\alpha+\beta q}{q}\right)^{-1/2} \exp\left[-\theta\left(\frac{q^2+\alpha+\beta q}{q}\right)^{1/2}\right] \tag{23}$$

where $\theta = x/K^{1/2}$, $q = p + (\chi^2/\tau)$, $\alpha = -\chi^2/\tau^2$ and $\beta = [(1-\chi^2)/\tau] + (U^2/4K)$

From (23):

$$C.\frac{2AK^{1/2}}{M}e^{-Ux/2K} = L^{-1}\left\{\left(\frac{q^2+\alpha+\beta q}{q}\right)^{-1/2} \exp\left[-\theta\left(\frac{q^2+\alpha+\beta q}{q}\right)^{1/2}\right]\right\}$$

The problem is now to find the inverse Laplace transform on the right hand side of (24). Eqn. (25) is derived from a standard form by differentiation (Roberts and Kaufmann (1966) p. 8 no. 62):

$$L\left\{\int_0^t f(v)\frac{(\alpha v)^{1/2}}{(t-v)^{1/2}}\mathcal{J}_{-1}[2(\alpha v)^{1/2}(t-v)^{1/2}]dv\right\} = \tilde{f}\left(p + \frac{\alpha}{p}\right) - \tilde{f}(p) \tag{25}$$

α is a constant and f is a function whose Laplace transform is $\tilde{f}$. Substituting $q = p + s$ and applying the translation theorem to (25) gives,

$$e^{-st}\{Int\} = L^{-1}\left\{\tilde{f}(q + \frac{\alpha}{q})\right\} - e^{-st}\cdot f(t) \tag{26}$$

where $\{Int\}$ is the bracketed integral on the LHS of (25). Now define the function f as,

$$f(t) = e^{-\beta t}\cdot e^{-\theta^2/4t}\cdot(\pi t)^{1/2} \tag{27}$$

where θ and β are constants. The Laplace transform of (27) is,

$$L(f(t)) = \frac{e^{-\theta\sqrt{p+\beta}}}{\sqrt{p+\beta}} = \tilde{f}(p+\beta) \tag{28}$$

which defines the Laplacian $\tilde{f}$ in the RHS of (26) if $f(t)$ is replaced by (27). For consistency (26) must now be written,

$$L^{-1}\left\{(q + \frac{\alpha}{q} + \beta)^{1/2}\exp\left[-\theta(q + \frac{\alpha}{q} + \beta)^{1/2}\right]\right\} = e^{-st}e^{-\beta t}e^{-\theta^2/4t}\cdot(\pi t)^{1/2} + e^{-st}\{Int\}, \tag{29}$$

which is the desired inverse transform. With the integral $\{Int\}$ expanded from (25), and (27) applied to $f(v)$, rearrangement of (24) gives:

$$C = \frac{M}{2AK^{1/2}}e^{Ux/2K}\left[\begin{array}{l} e^{-st}e^{-\beta t}e^{-\theta^2/4t}\cdot(\pi t)^{-1/2} + \\ e^{-st}\int_0^t e^{-\beta t}e^{-\theta^2/4t}(\pi t)^{-1/2}(\alpha v)^{1/2} \\ \quad (t-v)^{-1/2}\mathcal{J}_{-1}[2(\alpha v)^{1/2} \\ \quad\quad (t-v)^{-1/2}]dv \end{array}\right] \tag{30}$$

Equation (12) in the main text can easily be derived from (30) by substituting appropriate combinations of x, U, K, χ and τ for the parameters s, α, β and θ. Use is also made of the relations $\mathcal{J}_{-1} = -\mathcal{J}_1$ and $\mathcal{J}(iz) = -i\,I_1(z)$.

Finally, if the LHS of (2) is designated as $C_T(x,t)$ then (12) may be written in a simplified form,

$$C = C_T(x,t)e^{-t/\tau} + e^{-\chi^2 t/\tau}\int_0^t C_T(x,v).e^{\chi^2 v/\tau}.\frac{\chi}{\tau}.e^{-U/\tau} \cdot\frac{\sqrt{v}}{\sqrt{t-v}}.I_1\left[2\frac{\chi}{\tau}\sqrt{v(t-v)}\right].dv \tag{31}$$

which shows clearly how the first term represents tracer which has never entered dead zones, whereas the second

term represents tracer particles that have resided in dead zones at least once.

Appendix B: Previous models of mathematically related systems

Natural channels with dead zones are just one example of a class of phenomena in which a fluid moves through a region in which tracer is dispersed according to Fick's Law, but can also be exchanged with an adjacent region of immobile fluid, with a first-order rate equation governing the exchange. Examples occur in chromatography, Raschig reaction towers, and porous media containing blind pores, as well as porous media in which tracer undergoes linear, reversible sorption. Mathematically, all these systems have strong similarities. Solutions to Eqns. (6) and (7) have been presented for various boundary conditions by Coats and Smith (1964), Lapidus and Amundson (1952), De Smedt and Wierenga (1979a, b) and Carnahan and Remer (1984), among others, but do not include the particular solution presented here. However, the model of Raschig towers by Villermaux and Van Swaaij (1969) uses a Dirac delta function to represent an initial input of a chemical, and differs mathematically from the present model only in their choice of boundary condition at $x = 0$, $t = 0$. In this model, dispersion occurs only after the tracer has been advected into the test reach (Eqn. (9)), whereas Villermaux' and Van Swaaij's tracer may enter the test reach by forwards dispersion from a non-reactive reach upstream. Villermaux and Van Swaaij (1969) provide a useful discussion of the properties of their solution, which shows the same general features as our model.

Analytical derivation of solutions by the Laplace transform method can be achieved only for a few, tractable cases. Models such as the present one can now be produced in a workable form for a great variety of input conditions by using numerical methods of Laplace transform inversion (e.g. Barker, 1982; Moench, 1989, 1991).